The impact of unimolecular reactions on acyl peroxy radical initiated isoprene oxidation

Ida Karppinen[1], Dominika Pasik[1,2], Emelda Ahongshangbam[1,2], and Nanna Myllys[1,2]

[1]Department of Chemistry, University of Helsinki, Helsinki, 00014, Finland
[2]Institute for Atmospheric and Earth System Research, University of Helsinki, Helsinki, 00014, Finland

Correspondence: Nanna Myllys (nanna.myllys@helsinki.fi)

Abstract. The unimolecular H-shift and endoperoxide ring formation reactions were studied for several different acyl peroxy radicals (APRs) using quantum-mechanical methods. Also, for structures with slow unimolecular reactions, accretion reactions with isoprene were investigated. The goal of the study was to determine which APRs could work as atmospheric oxidants of unsaturated hydrocarbons. The reaction rate coefficients were calculated at the DLPNO-CCSD(T)/aug-cc-pVTZ//ωB97X-D/6-31+G* level using multi-conformer transition state theory. Unimolecular reactions of acyl peroxy radicals were shown to have rate coefficients up to 0.1 s^{-1} and bimolecular accretion reactions with isoprene up to 10^{-15} cm^{3}s^{-1}. Both smaller and larger acyl peroxy radicals with rigid structures were observed to be more likely to initiate oxidation of isoprene because of their inability for fast unimolecular reactions. The pseudo-first-order reaction rates were calculated for accretion reactions of isoprene with OH and six APRs at different temperatures. The significance of APR-initiated isoprene oxidation was shown to increase with increasing temperature. APR-initiated oxidation could lead to dimeric products with atmospheric impact through formation of low volatility compounds.

1 Introduction

Peroxy radicals (RO$_2$) can undergo a variety of different reactions in the atmosphere. RO$_2$ reactions with NO$_x$ and NO$_3$ are important in moderately to highly polluted conditions, however in clean environments, reactions with other species, mainly HO$_2$, become more significant (Jenkin et al., 2019). Unimolecular reactions, such as H-shift reactions and endoperoxide ring formation reactions, are also possible reaction pathways for RO$_2$ radicals. An interesting class of RO$_2$ radicals are acyl peroxy radicals (APRs), which have shown to be more reactive than other RO$_2$ radicals (Knap and Jørgensen, 2017; Seal et al., 2023; Møller et al., 2019; Vereecken and Nozière, 2020; Nozière and Fache, 2021). APRs are generally formed from aldehydes when the aldehydic hydrogen atom is removed by photolysis or in a reaction with the OH radical (Demore et al., 1997; Atkinson et al., 1997). In these reactions, an acyl radical forms and rapidly reacts with O$_2$ forming an APR (Atkinson and Arey, 2003). They can also be formed by photolysis of ketones (El-Agamey and McGarvey, 2002) or indirectly from aldehydes through a process called autoxidation (Crounse et al., 2013; Knap and Jørgensen, 2017). However, the direct APR formation route from aldehydes is the dominant one, since the removal of an aldehydic H atom is much faster than the removal of a non-aldehydic H atom (Calvert et al., 2011).

Studies have shown that APRs, unlike other RO_2 radicals, are enough reactive towards double bonds that these reactions can occur under atmospheric conditions (Nozière and Fache, 2021; Pasik et al., 2024a). Experimental studies of RO_2 gas-phase reactions with alkenes in high temperatures have also shown that APRs are more reactive towards double bonds than other RO_2 (Stark, 1997). Accretion reaction of an APR to an unsaturated hydrocarbon leads to a dimeric product with an alkyl radical center (Nozière et al., 2023). O_2 can add to this radical center forming new RO_2 radicals which may undergo autoxidation. The APR-initiated oxidation described leads to compounds with high molecular mass and multiple oxygen atoms. These compounds have low vapor pressure and therefore can potentially participate in atmospheric new-particle formation (NPF). NPF accounts for a major part of tropospheric aerosol production which can act as cloud condensation nuclei (CCN) and also negatively affect human health (Lee et al., 2019). However, it has also been found that APRs may go through fast H-shift reactions (Knap and Jørgensen, 2017; Møller et al., 2019; Vereecken and Nozière, 2020; Seal et al., 2023) making their reactions with unsaturated hydrocarbons less likely. Also, APRs with a double bond in the structure can go through endoperoxide ring formation reactions (Vereecken et al., 2021; Nozière and Vereecken, 2024). These reactions have been studied for RO_2 radicals and shown to compete with H-shift reactions (Vereecken and Peeters, 2004; Xu et al., 2019; Møller et al., 2020). Vereecken et al. (2021) also studied some APR ring closure reactions and showed that APR exhibits faster ring closure reactions compared to RO_2 radicals.

The unimolecular H-shift and ring closure reactions of APR leads to the formation of an alkyl radical to which O_2 rapidly adds forming a peroxy radical. It means that if APR undergoes fast unimolecular reactions, it cannot react with unsaturated hydrocarbons. Therefore, these unimolecular reactions have to be slow enough to allow accretion reactions to double bond which has been illustrated in Figure 1. Previous studies on unimolecular reactions of APRs have mainly focused on which of these reactions are fast in atmospheric conditions. The aim of this study is to find APR structures with slow ($k_{\text{uni}} \leq 10^{-4}\text{s}^{-1}$) unimolecular reactions but fast ($k_{\text{bi}} > 10^{-17}\text{cm}^3\text{s}^{-1}$) bimolecular accretion reactions to double bond. Our goal is to determine what type of APRs could work as oxidants of unsaturated hydrocarbons and initiate the formation of low volatility compounds. These APRs with slow unimolecular reactions and fast bimolecular accretion reactions to double bond are potential oxidants of unsaturated hydrocarbons. Hydroxyl radical (OH) accounts for 66-95 % of isoprene oxidaton (Gu et al., 2022), and therefore, the APR-initiated oxidation rate is compared to that of OH. Moreover, the temperature dependence of the bimolecular reactions is investigated, and the pseudo-first-order reaction rate coefficients are presented at different temperatures.

2 Methods

2.1 Computational details

Transition state (TS) structures were obtained using the relaxed potential energy surface (PES) scan using density functional theory (DFT) level ωB97X-D/6-31+G* (Chai and Head-Gordon, 2008b, a; Hehre et al., 1972; Clark et al., 1983). For unimolecular reactions, TS structures were located starting from the reactant, whereas for bimolecular reactions, they were located starting from the product. Prior to the PES scan, the reactant and product structures were optimized at the ωB97X-D/6-31+G* level of theory. Reactant and TS conformers were found using the CREST sampling tool at the GFN2-xTB level (Pracht et al.,
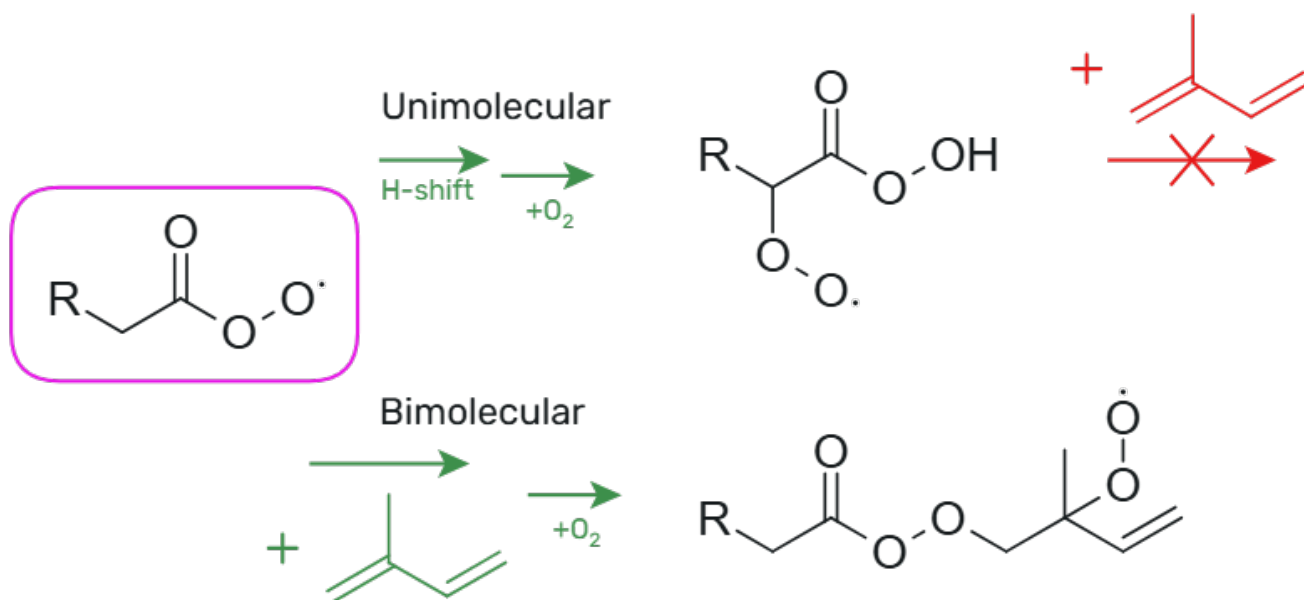
Figure 1. Possible reaction pathways for acyl peroxy radicals.

2020; Bannwarth et al., 2019). TS conformer configurational search included constraining the bonds forming the TS structure. For unimolecular H-shift reactions, this involved constraining the C−H and H−O bond distances, while for endoperoxide ring formation reactions, the O−C bond being formed was constrained. For bimolecular reactions the C−O bond being broken was kept constrained. Reactant and TS conformers were optimized at the same DFT level as previously, using a 2.5 kcal/mol cutoff after the CREST configurational search, as xTB level electronic energies correlate well with DFT energies (Pasik et al., 2024b; Kubečka et al., 2019). Duplicates were removed based on electronic energy and dipole moment, and TS structures were confirmed by one imaginary frequency. For the lowest energy reactant and TS structures, single point energies were calculated using the DLPNO-CCSD(T)/aug-cc-pVTZ level of theory (Riplinger and Neese, 2013; Riplinger et al., 2013; Dunning Jr, 1989; Kendall et al., 1992). All DFT calculations were carried out using Gaussian 16 software, and ORCA version 5.0.3 was used for the single-point energy calculations (Frisch et al., 2016; Neese, 2012).

To compare the significance of APR-initiated isoprene oxidation to that of OH, we performed calculations for the reactions between isoprene and OH as well. The TS structures for the bimolecular reactions between OH and isoprene could not be found with the ωB97X-D functional. This is because the saddle point is very shallow or might not even exist (see Supplementary Information Figures S2 and S3 for PES graphs). In addition, the pre-reactive complex that forms in the reaction is close in energy with the TS structure further explaining why the TS is difficult to locate (see Supplementary Information Figure S4 for energy diagrams). Thus, alternatively, the M06-2X functional was used (Zhao and Truhlar, 2008), and all reactant and TS conformers were optimized at the M06-2X/6-31+G* level for the reactions between OH and isoprene. On top of that, single-

point energies were calculated for the lowest energy conformers using the DLPNO-CCSD(T)/aug-cc-pVTZ level of theory. Three of the studied bimolecular reactions between isoprene and APRs (ace-APR reaction R4, pro-APR reaction R1, and ben-APR reaction R1) were additionally investigated at the DLPNO//M06-2X level to examine how the rate coefficients differ from those calculated at the DLPNO//ωB97X-D level. There is only a minor difference between zero-point corrected electronic energies at the studied DLPNO//DFT levels. However, partition functions between those density functionals differ significantly, which can affect an order of magnitude difference in rate coefficients. The results from these benchmark calculations are provided in the Supplementary Information (Table S2).

2.2 Rate coefficients

The multi-conformer transition state theory (MC-TST) was utilized to calculate the reaction rate coefficients (Vereecken and Peeters, 2003). The rate coefficients for the unimolecular reactions were calculated using Equation 1 (Møller et al., 2016).

$$k = \kappa_{\mathrm{t}} \frac{k_{\mathrm{B}}T}{h} \frac{\sum_i^{\text{allTSconf.}} \exp(-\frac{\Delta E_i}{k_{\mathrm{B}}T}) Q_{\mathrm{TS},i}}{\sum_j^{\text{allRconf.}} \exp(-\frac{\Delta E_j}{k_{\mathrm{B}}T}) Q_{\mathrm{R},j}} \exp(-\frac{E_{\mathrm{TS}} - E_{\mathrm{R}}}{k_{\mathrm{B}}T}), \tag{1}$$

where k_{B} is the Boltzmann's constant, T is the temperature and h is the Planck's constant. ΔE_i is the zero-point corrected energy of TS conformer i relative to the lowest energy TS conformer and $Q_{\mathrm{TS},i}$ is the partition function of TS conformer i both calculated at the ωB97X-D/6-31+G* level. ΔE_j and $Q_{\mathrm{R},j}$ are the analogous values for the reactant conformers. E_{TS} and E_{R} are the zero-point corrected energies of the lowest energy TS and reactant conformer, respectively, including the DLPNO-CCSD(T)/aug-cc-pVTZ correction.

κ_{t} is the quantum-mechanical tunneling coefficient which was calculated using the one-dimensional Eckart tunneling method (Eckart, 1930; Johnston and Heicklen, 1962). Tunneling was needed for H-shift reactions due to the low mass of the hydrogen atom (McMahon, 2003). To calculate the tunneling coefficient, forward and reverse intrinsic reaction coordinate (IRC) calculations were carried out to connect the lowest energy TS to the corresponding reactant and product (Møller et al., 2016). The resulting reactant and product structures were optimized at the ωB97X-D/6-31+G* level followed by DLPNO-CCSD(T)/aug-cc-pVTZ energy corrections. Additionally, the imaginary frequency of the lowest energy TS was utilized to calculate the tunneling coefficient.

The rate coefficients for the bimolecular reactions were calculated using Equation 2 (Viegas, 2018, 2021).

$$k = \kappa_{\mathrm{t}} \frac{k_{\mathrm{B}}T}{h P_{\mathrm{ref}} Q_{\mathrm{ip}}} \frac{\sum_i^{\text{allTSconf.}} \exp(-\frac{\Delta E_i}{k_{\mathrm{B}}T}) Q_{\mathrm{TS},i}}{\sum_j^{\text{allRconf.}} \exp(-\frac{\Delta E_j}{k_{\mathrm{B}}T}) Q_{\mathrm{R},j}} \exp(-\frac{E_{\mathrm{TS}} - E_{\mathrm{R}}}{k_{\mathrm{B}}T}), \tag{2}$$

where P_{ref} is the reference pressure ($= 2.45 \times 10^{19}$ molecules cm^{-3}) and Q_{ip} is the partition function of isoprene. The second isoprene conformer is 1.5 kcal/mol higher in energy than the lowest energy conformer which would lead to a small exponential
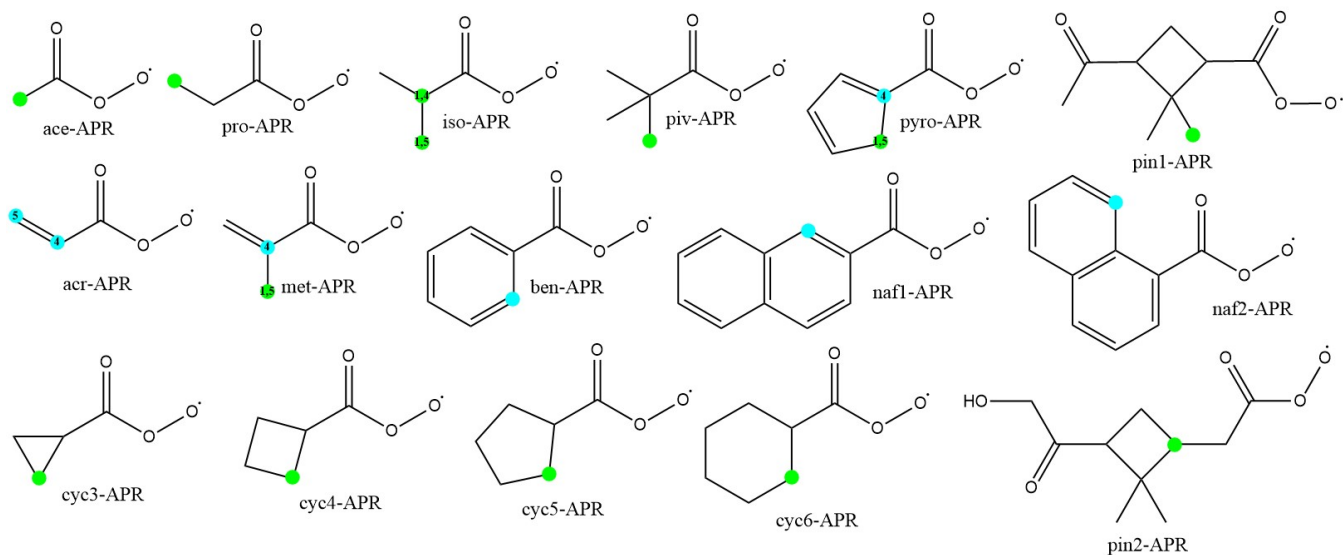
Figure 2. The chemical structures of acyl peroxy radicals investigated in this study. The fastest unimolecular reactions are marked with dots, green for H-shifts and blue for endoperoxide ring formations. For clarification, the prefixes for structures with two reactions with similar rates are also marked.

factor of 0.08 in Eq. 2 and a small contribution to the overall rate. Therefore, only the partition function of the lowest energy conformer of isoprene was considered in Eq. 2.

3 Results

105 The rates of unimolecular H-shift and endoperoxide ring formation reactions for several different APR structures are calculated. In addition, for structures exhibiting slow unimolecular reaction rates, bimolecular accretion reactions with isoprene are investigated. The APR structures and their corresponding names used in this study are presented in Figure 2. These structures include not only small APRs but also larger cyclic APR structures that are potentially too rigid for fast unimolecular reactions.

3.1 Unimolecular reactions

We calculated the reaction rate coefficients for unimolecular H-shift and endoperoxide ring formation reactions. For clarity, Table 1 presents only the results for the fastest calculated rate coefficients. The fastest reactions are also illustrated in Figure 2. Other calculated rate coefficients can be found in the Supplementary Information (Table S1).

The slowest unimolecular reactions were observed for the smallest systems such as ace-APR and cyc3-APR. The optimiza-
115 tion of the TS structure for the 1,4 H-shift reaction of ace-APR turned out to be difficult. A decomposition of the product results in the formation of ethenone and hydroperoxy radical during the optimization, making it difficult to find the correct TS. This

Table 1. Calculated energy barrier heights (ΔE^{TS} in kcal/mol), Eckart tunneling coefficients (κ_{t}) for H-shifts and unimolecular MC-TST reaction rate coefficients (k_{uni} in s^{-1}) at 298 K of fastest unimolecular reactions for the studied APRs. The APRs that have slow ($k_{\text{uni}} \leq 10^{-4}$s^{-1}) unimolecular reactions are bolded.

Radical	Reaction	ΔE^{TS}	κ_{t}	k_{uni}
Ace-APR	1,4 H-shift	29.79	460	1.07×10^{-7}
Pro-APR	1,5 H-shift	24.61	100	4.49×10^{-5}
Iso-APR	1,4 H-shift	22.95	43	3.49×10^{-3}
	1,5 H-shift	22.99	87	2.92×10^{-3}
Piv-APR	1,5 H-shift	22.47	37	1.32×10^{-3}
Acr-APR	4-endoperoxide	22.75	-	3.15×10^{-5}
	5-endoperoxide	23.66	-	3.95×10^{-6}
Met-APR	1,5 H-shift	24.30	1249	1.61×10^{-3}
	4-endoperoxide	20.36	-	1.51×10^{-3}
Ben-APR	4-endoperoxide	24.80	-	1.94×10^{-6}
	5-endoperoxide	23.55	-	5.67×10^{-6}
Pyro-APR	1,5 H-shift	25.50	25302	4.77×10^{-3}
	4-endoperoxide	19.66	-	6.18×10^{-3}
Cyc6-APR	1,5 H-shift	19.95	14	5.06×10^{-2}
Cyc5-APR	1,5 H-shift	20.44	50	7.65×10^{-2}
Cyc4-APR	1,5 H-shift	22.62	43	1.46×10^{-3}
Cyc3-APR	1,5 H-shift	29.40	18	4.13×10^{-9}
Pin1-APR	1,6 H-shift	23.54	92	1.32×10^{-3}
Pin2-APR	1,5 H-shift	19.84	44	1.60×10^{-1}
Naf1-APR	5-endoperoxide	20.86	-	3.25×10^{-4}
Naf2-APR	6-endoperoxide	17.42	-	5.81×10^{-2}

decomposition channel of the product is presented in Figure 3. The reaction has also been studied in more detail by Sandhiya and Senthilkumar (2020). However, after several attempts, the correct TS structure was found and the correct rate coefficient was calculated for this H-shift reaction. For pyro-APR 1,5 H-shift a very large tunneling coefficient of 25302 was observed. A large imaginary frequency of $2238i$ cm^{-1} results in a large tunneling coefficient. This coefficient differs from other calculated tunneling coefficients significantly, which could suggest that the Eckart method may no longer be reliable in this case. The Eckart method is a very simple model compared to multidimensional models that also take into account other variables along the reaction path (Zhang and Dibble, 2011; Meana-Pañeda et al., 2011). However, for the purposes of this study using the Eckart method is reasonable due to the saved computational resources.

By increasing system size an increase in the unimolecular rate coefficients was observed which was to be expected. Larger system size allows H-shifts from further positions relative to the peroxy radical group resulting in a larger TS ring size with less
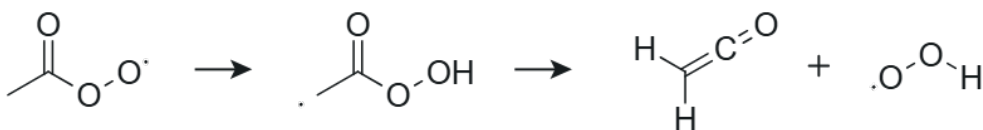
Figure 3. 1,4 H-shift reaction of ace-APR and the decomposition of the product.

strain. However, slower reactions were also observed for rigid systems, for example, ben-APR and naf1-APR. This is due to the rigid structure and aromaticity of the benzene ring which does not allow fast H-shift nor endoperoxide ring formation reactions. However, naf2-APR is capable of quite fast unimolecular reactions despite the rigid structure. By adjusting the position of the
130 APR group, a 6-endoperoxide ring formation reaction becomes possible, leading to the formation of a 6-membered ring product and facilitating a faster unimolecular reaction. A similar reaction mechanism is not efficient for naf1-APR, as the formation of the 6-membered ring is hindered.

Endoperoxide ring formations were found to be competitive with H-shift reactions or, in most cases, even faster. Vereecken et al. (2021) studied ring closure reactions and calculated rate coefficients for multiple different RO_2 radicals, including
135 $C_2H_3CH_2OO\cdot$, a non-acyl peroxy radical system similar to acr-APR. For $C_2H_3CH_2OO\cdot$, values of 4.6×10^{-11} s^{-1} and 2.3×10^{-10} s^{-1} were obtained for 4- and 5-endoperoxide reactions, respectively, in the study by Vereecken et al. (2021). The values obtained in this study for acr-APR are significantly higher compared to $C_2H_3CH_2OO\cdot$, suggesting that ring formation reactions are faster for APRs compared to other RO_2. Unexpectedly, 4-endoperoxide reactions for acr-, met-, and pyro-APR were faster than the 5-endoperoxide reactions. Contrastingly, according to values calculated by Vereecken et al. (2021) for
140 $C_2H_3CH_2OO\cdot$, the 5-endoperoxide reaction was faster than the 4-endoperoxide reaction. The TS structures of acr-APR 4- and 5-endoperoxide reactions are presented in Figure 4. Moreover, we did not observe any difference in allylic and non-allylic H-shift reactions when comparing iso- and met-APR 1,5 H-shifts. For other RO_2 radicals allylic H-shifts have been shown to be significantly faster than non-allylic H-shifts (Otkjær et al., 2018; Vereecken and Nozière, 2020). However, we have been unable to identify any reasons for these distinct behaviors of APRs compared to other RO_2 radicals.

145 **3.2 Bimolecular reactions**

Isoprene and peroxy radicals can react through four different pathways, where the peroxy radical adds to one of the four sp^2 carbons in isoprene. These four pathways are presented in Figure 5. Pasik et al. (2024b) studied these different pathways and showed that reaction pathways R1 and R4, where the peroxy radical adds to one of the two terminal sp^2 carbons, are the fastest. The reaction pathway R1 leads to a tertiary (allylic) radical and R4 to a secondary (allylic) radical which makes them faster
150 than reaction pathways R2 and R3 which lead to primary radicals. Therefore, only reaction pathways R1 and R4 were the focus of this study.

Of interest were the APR structures which had slow ($k_{uni} \leq 10^{-4}$s^{-1}) unimolecular reactions. In correspondence, six APR structures (ace-, pro-, acr-, ben-, cyc3-, and naf1-APR) were chosen for further calculations to study their bimolecular reactions
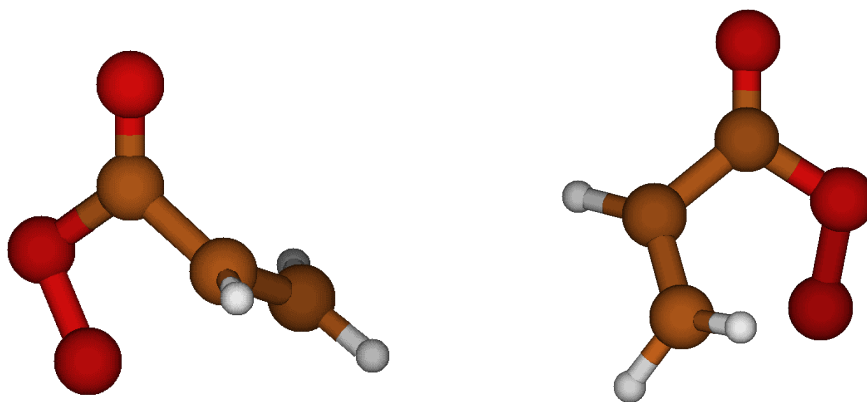
Figure 4. Transition state structures of acr-APR 4-endoperoxide (left) and 5-endoperoxide (right) ring formation reaction. Color coding: brown is carbon, red is oxygen, and white is hydrogen.
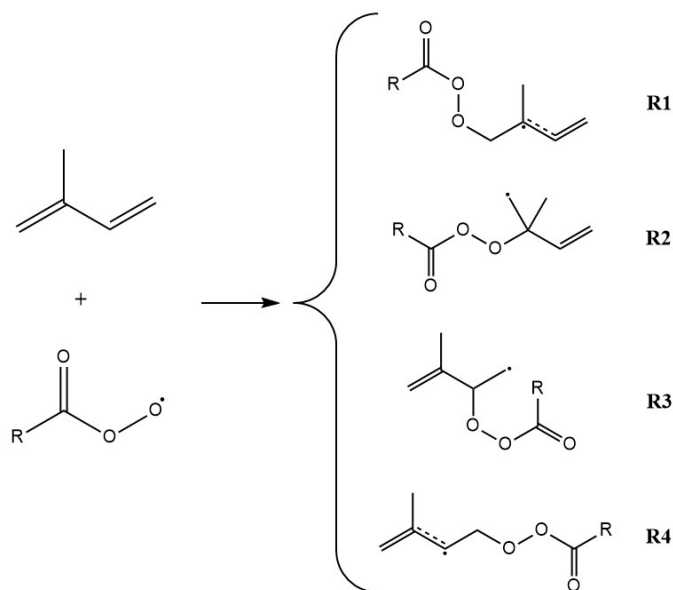
Figure 5. Reaction pathways for reaction between isoprene and acyl peroxy radical.

(see Table 1). The same reaction pathways were also studied for the reaction between isoprene and OH to assess the signif-
155 icance of APR-initiated oxidation of isoprene. Calculations on reactions between isoprene and APRs were carried out at the DLPNO-CCSD(T)/aug-cc-pVTZ//ωB97X-D/6-31+G* level and calculations for OH reactions at the DLPNO-CCSD(T)/aug-cc-pVTZ//M06-2X/6-31+G* level. Table 2 presents the calculated rate coefficients for both reaction pathways R1 and R4. The table also includes the forward reaction barrier heights and the total reaction rates which were assumed to be a sum of reaction rates R1 and R4.

Table 2. Calculated energy barrier heights (ΔE^{TS} in kcal/mol) and bimolecular MC-TST reaction rate coefficients (k_{bi} in $\mathrm{cm^3 s^{-1}}$) at 298 K for reactions R1 and R4 of isoprene with OH and APRs. Rates for APR and isoprene reactions were calculated at the DLPNO-CCSD(T)/aug-cc-pVTZ//ωB97X-D/6-31+G* level and for OH and isoprene reactions at the DLPNO-CCSD(T)/aug-cc-pVTZ//M06-2X/6-31+G* level. Total k_{bi} is the sum of reaction rates R1 and R4.

Radical	Reaction	ΔE^{TS}	k_{bi}	Total k_{bi}
Ace-APR	R1	1.8	1.2×10^{-16}	1.3×10^{-16}
	R4	2.8	1.1×10^{-17}	
Pro-APR	R1	1.3	1.3×10^{-16}	1.3×10^{-16}
	R4	2.3	9.5×10^{-18}	
Acr-APR	R1	0.4	7.1×10^{-16}	7.8×10^{-16}
	R4	1.4	7.4×10^{-17}	
Ben-APR	R1	0.1	1.6×10^{-15}	1.7×10^{-15}
	R4	1.0	1.2×10^{-16}	
Cyc3-APR	R1	0.6	2.2×10^{-16}	2.6×10^{-16}
	R4	1.6	3.3×10^{-17}	
Naf1-APR	R1	0.5	7.7×10^{-16}	9.9×10^{-16}
	R4	0.7	2.2×10^{-16}	
OH	R1	-2.5	3.2×10^{-11}	5.0×10^{-11}
	R4	-2.4	1.8×10^{-11}	

As expected, reaction pathway R1 is the fastest for all studied structures. This is explained by the reaction product having a tertiary resonance stabilised carbon-centered radical in comparison to reaction pathway R4 which leads to a secondary (allylic) radical. It can also be seen that the forward barrier decreases as reactant APR size increases. Unsaturated APR, acr-APR, also exhibits faster reactions with isoprene. These results align with observations made in other studies for APRs and other RO_2 radicals (Pasik et al., 2024b; Nozière and Fache, 2021). Unsaturated and large APRs could effectively stabilize the breaking of the π bond as the electron density can be delocalized over several atoms resulting in decreased barriers. An exception to this is naf1-APR reaction R1 which has a slightly larger barrier than the corresponding reaction of ben-APR despite the larger structure of naf1-APR reaction. However, the barrier for naf1-APR reaction R1 is still close to zero resulting in a relatively fast reaction.

The values for the three reactions of isoprene with ace-, pro-, and ben-APR calculated at the DLPNO-CCSD(T)/aug-cc-pVTZ//M06-2X/6-31+G* level are provided in the Supplementary Information (Table S2). The rate coefficients calculated with the M06-2X functional are smaller, up to approximately an order of magnitude smaller, compared to the ones calculated at the DLPNO-CCSD(T)/aug-cc-pVTZ//ωB97X-D/6-31+G* level. Therefore, the different levels of theory used in this study are not completely compatible with each other and make the comparison of OH- and APR-initiated isoprene oxidation more

difficult. However, reasonable conclusions can be made from the results and the impact of APR-initiated oxidation of isoprene can be assessed.

Nozière and Fache (2021) obtained an experimental value of 2×10^{-14} cm^3 s^{-1} for the reaction between ace-APR and isoprene. In the same study, a Structure-Activity-Relationship (SAR) recommended by Stark (1997) was used to calculate a value of 4.1×10^{-15} cm^3 s^{-1} for the same reaction. Both rates are considerably higher than the total rate of 1.3×10^{-16} cm^3 s^{-1} calculated in this study. This would suggest that the rates calculated in this study underestimate the total bimolecular rates for reactions between APRs and isoprene. We are also underestimating the rate constant for OH reaction with isoprene. An experimental value of 1.0×10^{-10} cm^3 s^{-1} (Atkinson et al., 1997) has been obtained for the reaction between OH and isoprene which differs from our theoretical value by a factor of two. The value calculated in this study does not take into account the other two reaction pathways R2 and R3, which do also contribute to the rate coefficient. However, these contributions are minor, somewhere in the % range (Jenkin et al., 1998; Stevens et al., 2000). While we are underestimating the rates for these reactions, the comparison between OH- and APR-initiated isoprene oxidation should be reliable.

The change of bimolecular reaction rates as a function of temperature was also investigated at the same levels of theory as the initial calculations. Rate coefficients were calculated at four different temperatures (248 K, 273 K, 298 K, and 323 K) and the total bimolecular rates were again assumed to be a sum of reaction rates R1 and R4. The pseudo-first-order reaction rates were calculated from the total bimolecular rates using a concentration of 10^6 cm^{-3} for OH (Wennberg et al., 2018) and a concentration of 10^8 cm^{-3} for all APRs. The APR concentration used is a mean value of ace-APR concentration in hydrocarbon-rich remote atmospheres under low NO$_x$ conditions from a study by Villenave et al. (1998). Data on other APR concentrations could not be obtained and the ace-APR concentration was used as a default concentration for all other APRs. This assumption leads to some uncertainty in the results but they can be assumed to be an upper limit for the pseudo-first-order rates. The results are provided in Table 3. An increase in the pseudo-first-order rates for the APR reactions can be observed as temperature increases. On the contrary, a decrease in the pseudo-first-order rate of reaction between isoprene and OH can be distinguished as temperature increases. The negative temperature dependence of OH-initiated oxidation of isoprene has also been observed in experimental studies (Dillon et al., 2017; Kleindienst et al., 1982). This difference in the temperature dependence can be attributed to differences in the barriers. The addition of OH to isoprene has a negative barrier, whereas APR additions have positive barriers. This leads to a larger impact of APR-initiated oxidation of isoprene compared to that of OH at higher temperatures. At 248 K APRs could be responsible for up to 0.1% of isoprene oxidation compared to OH-initiated isoprene oxidation and at 323 K the significance of APR-initiated oxidation could be up to 1%.

4   Conclusions

We investigated unimolecular H-shift and endoperoxide ring formation reactions for a variety of acyl peroxy radicals using quantum-mechanical methods. The goal of this study was to determine which APRs could work as atmospheric oxidants of unsaturated hydrocarbons. We selected 16 APR structures with different functionalities and found six APRs with slow unimolecular reactions making them potential oxidants of alkenes. As expected, many of the studied APRs had quite fast

Table 3. Calculated pseudo-first-order reaction rates (k_{pseudo}[radical] in $\text{cm}^{-3}\text{s}^{-1}$) for studied reactions of isoprene with OH and APRs in four different temperatures (T in K). Concentrations of 10^6 molecules cm^{-3} and 10^8 molecules cm^{-3} were used for OH and all APRs, respectively.

T	k_{pseudo}[Ace-APR]	k_{pseudo}[Pro-APR]	k_{pseudo}[Acr-APR]	k_{pseudo}[Ben-APR]	k_{pseudo}[CycPro-APR]	k_{pseudo}[Naf1-APR]	k_{pseudo}[OH]
248	5.9×10^{-9}	7.3×10^{-9}	5.2×10^{-8}	1.3×10^{-7}	1.6×10^{-8}	6.4×10^{-8}	1.2×10^{-4}
273	9.1×10^{-9}	1.0×10^{-8}	6.4×10^{-8}	1.5×10^{-7}	2.1×10^{-8}	8.1×10^{-8}	7.5×10^{-5}
298	1.3×10^{-8}	1.3×10^{-8}	7.8×10^{-8}	1.7×10^{-7}	2.6×10^{-8}	9.9×10^{-8}	5.0×10^{-5}
323	1.9×10^{-8}	1.8×10^{-8}	9.5×10^{-8}	2.0×10^{-7}	3.2×10^{-8}	1.2×10^{-7}	3.6×10^{-5}

unimolecular reactions, up to 0.1 s^{-1}. However, we found several APRs with low unimolecular reaction rate coefficients. For instance, small ace- and pro-APRs have reaction rate constants in the order of 10^{-7} and 10^{-5} s^{-1}, respectively. An even slower reaction was observed for a rigid APR with a 3-membered ring, cyc3-APR, for which the reaction rate constant was found to be as low as 10^{-9} s^{-1}. For aromatic structures, the endoperoxide ring formation was faster than the H-shift reaction, but due to rigid structure and aromaticity, the reaction rate constants were still low, in order of 10^{-5} s^{-1} for ben-APR and 10^{-4} s^{-1} for naf1-APR. Another naphthalene structure, naf2-APR, was able to form a 6-membered endoperoxide ring, and therefore, the unimolecular endoperoxide ring formation reaction was fast. Generally, where endoperoxide ring formation reactions were possible, they were shown to be competitive with H-shift reactions, and in most cases even faster.

Bimolecular accretion reactions between isoprene and APRs were also investigated in this study. Six APRs with slow unimolecular reactions were chosen for further calculations. Two pathways producing an allylic radical, R1 and R4, were studied for reactions between isoprene and the APRs. Pathway R1 was proven to be faster due to the formation of a tertiary allylic radical. Quite consistently, the reaction barrier heights decreased as system size increased for both pathways. The temperature dependence of these reactions was also studied and compared to OH-initiated isoprene oxidation. We calculated the pseudo-first-order reaction rates for isoprene oxidation initiated by OH and six APRs at four different temperatures. For all studied APRs, the reaction rate increased as temperature increased, whereas in the case of OH, the reaction rate decreased as temperature increased. This indicates a larger impact of APR-initiated isoprene oxidation compared to that of OH at higher temperatures. At 323 K, APRs could be responsible for up to 1% of isoprene oxidation in the atmosphere compared to OH. While the percentage of APR-initiated oxidation of isoprene compared to OH is not significant, APR-initiated oxidation can directly lead to high molar mass dimeric products. These dimeric compounds with multiple oxygen atoms and high molar mass have low vapor pressure, and therefore, they are candidates to participate in new-particle formation and growth. Thus, despite the minor contribution to initiate oxidation of isoprene, APRs might have an important role in producing low-volatility organic compounds from reactions with other unsaturated hydrocarbons, such as monoterpenes. For a better understanding of the impact of APR-initiated oxidation, measurements contributing to APR concentrations in the atmosphere are needed.

230   *Data availability.*   The optimized structures and calculation output files of all relevant compounds that support the findings of this manuscript will be available in the Zenodo repository.

Author contributions.   IK performed the calculations and wrote the manuscript. DP and EA assisted with the calculations. DP and NM contributed to the analysis. The study was designed and supervised by NM. All authors proofread the manuscript.

Competing interests.   The authors declare that they have no conflict of interests.

235   *Acknowledgements.*   We acknowledge the Research Council of Finland for funding (grant nos. 347775) and the CSC-IT Center for Science in Espoo, Finland, for computational resources. DP thanks the Doctoral Programme in Atmospheric Sciences (ATM-DP) at the University of Helsinki for providing funding.

References

Atkinson, R. and Arey, J.: Atmospheric degradation of volatile organic compounds, Chemical reviews, 103, 4605–4638, 2003.

240 Atkinson, R., Baulch, D., Cox, R., Hampson Jr, R., Kerr, J., Rossi, M., and Troe, J.: Evaluated kinetic, photochemical and heterogeneous data for atmospheric chemistry: Supplement V. IUPAC Subcommittee on Gas Kinetic Data Evaluation for Atmospheric Chemistry, Journal of Physical and Chemical Reference Data, 26, 521–1011, 1997.

Bannwarth, C., Ehlert, S., and Grimme, S.: GFN2-xTB—An accurate and broadly parametrized self-consistent tight-binding quantum chemical method with multipole electrostatics and density-dependent dispersion contributions, Journal of chemical theory and computation,

245 15, 1652–1671, 2019.

Calvert, J., Mellouki, A., Orlando, J., Pilling, M., and Wallington, T.: Mechanisms of Atmospheric Oxidation of the Oxygenates, Oxford University Press USA, ISBN 9780199767076, 2011.

Chai, J.-D. and Head-Gordon, M.: Long-range corrected hybrid density functionals with damped atom–atom dispersion corrections, Physical Chemistry Chemical Physics, 10, 6615–6620, 2008a.

250 Chai, J.-D. and Head-Gordon, M.: Systematic optimization of long-range corrected hybrid density functionals, The Journal of chemical physics, 128, 2008b.

Clark, T., Chandrasekhar, J., Spitznagel, G. W., and Schleyer, P. V. R.: Efficient diffuse function-augmented basis sets for anion calculations. III. The 3-21+ G basis set for first-row elements, Li–F, Journal of Computational Chemistry, 4, 294–301, 1983.

Crounse, J. D., Nielsen, L. B., Jørgensen, S., Kjaergaard, H. G., and Wennberg, P. O.: Autoxidation of organic compounds in the atmosphere,

255 The Journal of Physical Chemistry Letters, 4, 3513–3520, 2013.

Demore, W., Sander, S., Golden, D., Hampson, R., Kurylo, M., Howard, C., Ravishankara, A., Kolb, C., and Molina, M.: Chemical Kinetics and Photochemical Data for Use in Stratospheric Modeling, JPL Publication, 90, 1997.

Dillon, T. J., Dulitz, K., Groß, C., and Crowley, J. N.: Temperature-dependent rate coefficients for the reactions of the hydroxyl radical with the atmospheric biogenics isoprene, alpha-pinene and delta-3-carene, Atmospheric Chemistry and Physics, 17, 15 137–15 150, 2017.

260 Dunning Jr, T. H.: Gaussian basis sets for use in correlated molecular calculations. I. The atoms boron through neon and hydrogen, The Journal of chemical physics, 90, 1007–1023, 1989.

Eckart, C.: The penetration of a potential barrier by electrons, Physical Review, 35, 1303, 1930.

El-Agamey, A. and McGarvey, D. J.: Acyl/aroylperoxyl radicals: a comparative study of the reactivity of peroxyl radicals resulting from the α-cleavage of ketones, Physical Chemistry Chemical Physics, 4, 1611–1617, 2002.

265 Frisch, M. J., Trucks, G. W., Schlegel, H. B., Scuseria, G. E., Robb, M. A., Cheeseman, J. R., Scalmani, G., Barone, V., Petersson, G. A., Nakatsuji, H., Li, X., Caricato, M., Marenich, A. V., Bloino, J., Janesko, B. G., Gomperts, R., Mennucci, B., Hratchian, H. P., Ortiz, J. V., Izmaylov, A. F., Sonnenberg, J. L., Williams-Young, D., Ding, F., Lipparini, F., Egidi, F., Goings, J., Peng, B., Petrone, A., Henderson, T., Ranasinghe, D., Zakrzewski, V. G., Gao, J., Rega, N., Zheng, G., Liang, W., Hada, M., Ehara, M., Toyota, K., Fukuda, R., Hasegawa, J., Ishida, M., Nakajima, T., Honda, Y., Kitao, O., Nakai, H., Vreven, T., Throssell, K., Montgomery, Jr., J. A., Peralta, J. E., Ogliaro, F.,

270 Bearpark, M. J., Heyd, J. J., Brothers, E. N., Kudin, K. N., Staroverov, V. N., Keith, T. A., Kobayashi, R., Normand, J., Raghavachari, K., Rendell, A. P., Burant, J. C., Iyengar, S. S., Tomasi, J., Cossi, M., Millam, J. M., Klene, M., Adamo, C., Cammi, R., Ochterski, J. W., Martin, R. L., Morokuma, K., Farkas, O., Foresman, J. B., and Fox, D. J.: Gaussian 16 Revision C.02, gaussian Inc. Wallingford CT, 2016.

Gu, C., Wang, S., Zhu, J., Wu, S., Duan, Y., Gao, S., and Zhou, B.: Investigation on the urban ambient isoprene and its oxidation processes, Atmospheric Environment, 270, 118 870, 2022.

275   Hehre, W. J., Ditchfield, R., and Pople, J. A.: Self—consistent molecular orbital methods. XII. Further extensions of Gaussian—type basis sets for use in molecular orbital studies of organic molecules, The Journal of Chemical Physics, 56, 2257–2261, 1972.

Jenkin, M. E., Boyd, A. A., and Lesclaux, R.: Peroxy radical kinetics resulting from the OH-initiated oxidation of 1, 3-butadiene, 2, 3-dimethyl-1, 3-butadiene and isoprene, Journal of Atmospheric Chemistry, 29, 267–298, 1998.

Jenkin, M. E., Valorso, R., Aumont, B., and Rickard, A. R.: Estimation of rate coefficients and branching ratios for reactions of organic
280   peroxy radicals for use in automated mechanism construction, Atmospheric Chemistry and Physics, 19, 7691–7717, 2019.

Johnston, H. S. and Heicklen, J.: Tunnelling corrections for unsymmetrical Eckart potential energy barriers, The Journal of Physical Chemistry, 66, 532–533, 1962.

Kendall, R. A., Dunning, T. H., and Harrison, R. J.: Electron affinities of the first-row atoms revisited. Systematic basis sets and wave functions, The Journal of chemical physics, 96, 6796–6806, 1992.

285   Kleindienst, T. E., Harris, G. W., and Pitts, J. N.: Rates and temperature dependences of the reaction of hydroxyl radical with isoprene, its oxidation products, and selected terpenes, Environmental Science & Technology, 16, 844–846, 1982.

Knap, H. C. and Jørgensen, S.: Rapid hydrogen shift reactions in acyl peroxy radicals, The Journal of Physical Chemistry A, 121, 1470–1479, 2017.

Kubečka, J., Besel, V., Kurtén, T., Myllys, N., and Vehkamaki, H.: Configurational sampling of noncovalent (atmospheric) molecular clusters:
290   sulfuric acid and guanidine, The Journal of Physical Chemistry A, 123, 6022–6033, 2019.

Lee, S.-H., Gordon, H., Yu, H., Lehtipalo, K., Haley, R., Li, Y., and Zhang, R.: New particle formation in the atmosphere: From molecular clusters to global climate, Journal of Geophysical Research: Atmospheres, 124, 7098–7146, 2019.

McMahon, R. J.: Chemical reactions involving quantum tunneling, Science, 299, 833–834, 2003.

Meana-Pañeda, R., Truhlar, D. G., and Fernández-Ramos, A.: High-level direct-dynamics variational transition state theory calculations
295   including multidimensional tunneling of the thermal rate constants, branching ratios, and kinetic isotope effects of the hydrogen abstraction reactions from methanol by atomic hydrogen, The Journal of chemical physics, 134, 2011.

Møller, K. H., Otkjær, R. V., Hyttinen, N., Kurte´n, T., and Kjaergaard, H. G.: Cost-effective implementation of multiconformer transition state theory for peroxy radical hydrogen shift reactions, The Journal of Physical Chemistry A, 120, 10 072–10 087, 2016.

Møller, K. H., Bates, K. H., and Kjaergaard, H. G.: The importance of peroxy radical hydrogen-shift reactions in atmospheric isoprene
300   oxidation, The Journal of Physical Chemistry A, 123, 920–932, 2019.

Møller, K. H., Otkjær, R. V., Chen, J., and Kjaergaard, H. G.: Double bonds are key to fast unimolecular reactivity in first-generation monoterpene hydroxy peroxy radicals, The Journal of Physical Chemistry A, 124, 2885–2896, 2020.

Neese, F.: The ORCA program system, Wiley Interdisciplinary Reviews: Computational Molecular Science, 2, 73–78, 2012.

Nozière, B. and Fache, F.: Reactions of organic peroxy radicals, RO 2, with substituted and biogenic alkenes at room temperature: unsuspected
305   sinks for some RO 2 in the atmosphere?, Chemical Science, 12, 11 676–11 683, 2021.

Nozière, B. and Vereecken, L.: H-shift and cyclization reactions in unsaturated alkylperoxy radicals near room temperature: propagating or terminating autoxidation?, Physical Chemistry Chemical Physics, 26, 25 373–25 384, 2024.

Nozière, B., Durif, O., Dubus, E., Kylington, S., Emmer, Å., Fache, F., Piel, F., and Wisthaler, A.: The reaction of organic peroxy radicals with unsaturated compounds controlled by a non-epoxide pathway under atmospheric conditions, Physical Chemistry Chemical Physics,
310   25, 7772–7782, 2023.

Otkjær, R. V., Jakobsen, H. H., Tram, C. M., and Kjaergaard, H. G.: Calculated hydrogen shift rate constants in substituted alkyl peroxy radicals, The Journal of Physical Chemistry A, 122, 8665–8673, 2018.

Pasik, D., Frandsen, B. N., Meder, M., Iyer, S., Kurtén, T., and Myllys, N.: Gas-Phase Oxidation of Atmospherically Relevant Unsaturated Hydrocarbons by Acyl Peroxy Radicals, Journal of the American Chemical Society, 146, 13 427–13 437, 2024a.

315 Pasik, D., Iyer, S., and Myllys, N.: Cost-effective approach for atmospheric accretion reactions: a case of peroxy radical addition to isoprene, Physical Chemistry Chemical Physics, 26, 2560–2567, 2024b.

Pracht, P., Bohle, F., and Grimme, S.: Automated exploration of the low-energy chemical space with fast quantum chemical methods, Physical Chemistry Chemical Physics, 22, 7169–7192, 2020.

Riplinger, C. and Neese, F.: An efficient and near linear scaling pair natural orbital based local coupled cluster method, The Journal of
320 chemical physics, 138, 2013.

Riplinger, C., Sandhoefer, B., Hansen, A., and Neese, F.: Natural triple excitations in local coupled cluster calculations with pair natural orbitals, The Journal of chemical physics, 139, 2013.

Sandhiya, L. and Senthilkumar, K.: Unimolecular decomposition of acetyl peroxy radical: a potential source of tropospheric ketene, Physical Chemistry Chemical Physics, 22, 26 819–26 827, 2020.

325 Seal, P., Barua, S., Iyer, S., Kumar, A., and Rissanen, M.: A systematic study on the kinetics of H-shift reactions in pristine acyl peroxy radicals, Physical Chemistry Chemical Physics, 25, 28 205–28 212, 2023.

Stark, M. S.: Epoxidation of alkenes by peroxyl radicals in the gas phase: structure- activity relationships, The Journal of Physical Chemistry A, 101, 8296–8301, 1997.

Stevens, P. S., Seymour, E., and Li, Z.: Theoretical and experimental studies of the reaction of OH with isoprene, The Journal of Physical
330 Chemistry A, 104, 5989–5997, 2000.

Vereecken, L. and Nozière, B.: H migration in peroxy radicals under atmospheric conditions, Atmospheric chemistry and physics, 20, 7429–7458, 2020.

Vereecken, L. and Peeters, J.: The 1, 5-H-shift in 1-butoxy: A case study in the rigorous implementation of transition state theory for a multirotamer system, The Journal of chemical physics, 119, 5159–5170, 2003.

335 Vereecken, L. and Peeters, J.: Nontraditional (per) oxy ring-closure paths in the atmospheric oxidation of isoprene and monoterpenes, The Journal of Physical Chemistry A, 108, 5197–5204, 2004.

Vereecken, L., Vu, G., Wahner, A., Kiendler-Scharr, A., and Nguyen, H.: A structure activity relationship for ring closure reactions in unsaturated alkylperoxy radicals, Physical Chemistry Chemical Physics, 23, 16 564–16 576, 2021.

Viegas, L. P.: Exploring the reactivity of hydrofluoropolyethers toward OH through a cost-effective protocol for calculating multiconformer
340 transition state theory rate constants, The Journal of Physical Chemistry A, 122, 9721–9732, 2018.

Viegas, L. P.: Simplified protocol for the calculation of multiconformer transition state theory rate constants applied to tropospheric OH-initiated oxidation reactions, The Journal of Physical Chemistry A, 125, 4499–4512, 2021.

Villenave, E., Lesclaux, R., Seefeld, S., and Stockwell, W. R.: Kinetics and atmospheric implications of peroxy radical cross reactions involving the CH3C (O) O2 radical, Journal of Geophysical Research: Atmospheres, 103, 25 273–25 285, 1998.

345 Wennberg, P. O., Bates, K. H., Crounse, J. D., Dodson, L. G., McVay, R. C., Mertens, L. A., Nguyen, T. B., Praske, E., Schwantes, R. H., Smarte, M. D., St Clair, J. M., Teng, A. P., Zhang, X., and Seinfeld, J. H.: Gas-phase reactions of isoprene and its major oxidation products, Chemical reviews, 118, 3337–3390, 2018.

Xu, L., Møller, K. H., Crounse, J. D., Otkjær, R. V., Kjaergaard, H. G., and Wennberg, P. O.: Unimolecular reactions of peroxy radicals formed in the oxidation of α-pinene and β-pinene by hydroxyl radicals, The Journal of Physical Chemistry A, 123, 1661–1674, 2019.

350   Zhang, F. and Dibble, T. S.: Impact of tunneling on hydrogen-migration of the n-propylperoxy radical, Physical Chemistry Chemical Physics, 13, 17 969–17 977, 2011.

Zhao, Y. and Truhlar, D. G.: The M06 suite of density functionals for main group thermochemistry, thermochemical kinetics, noncovalent interactions, excited states, and transition elements: two new functionals and systematic testing of four M06-class functionals and 12 other functionals, Theoretical chemistry accounts, 120, 215–241, 2008.